Cobalt-H₃BTC Metal Organic Framework Based Electrochemical Nanosensor for Hydrogen Peroxide

Mahdi Hesari^{1,3} Rui Jia, ^{1,2} Shu Wu, ^{1,2} and Michael V. Mirkin^{1,2,z}

¹Department of Chemistry and Biochemistry, Queens College, City University of New York, Flushing, New York 11367, United States

²The Graduate Center of CUNY, New York, New York 10016, United States

³Department of Chemistry, State University of New York at Oswego, Oswego, New York, 13126, United States

^ze-mail: mmirkin@qc.cuny.edu

Keywords: nanoelectrode, metal organic framework, carbon nanopipette, hydrogen peroxide, nanosensor.

Abstract

Metal organic frameworks (MOFs) have found diverse applications in electrocatalysis and electrochemical sensing, owing to the presence of both metallic nodes and organic networks. Here, we electrosynthesized cobalt benzene tricarboxylate MOF inside an open carbon nanopipette (CNP) to produce a CNP-CoMOF nanoelectrode whose response is determined by Co^(II)/Co^(III) nodes attached to its porous nanostructure. Steady-state voltammograms of ferrocenemethanol, at CNP-CoMOF nanoelectrodes exhibit a sigmoidal shape with a well-defined plateau current. A linear calibration curve obtained for the hydrogen peroxide oxidation suggests that CNP–CoMOF nanoelectrodes are potentially useful as nanosensors for peroxide free from interference of dissolved dioxygen.

Introduction

The fascinating physicochemical properties of metal—organic frameworks (MOFs) have resulted in a rapid progress in MOF syntheses and applications [1-4]. The combination of metal ions (nodes) with organic linkers has made MOFs an outstanding platform for various electrochemical applications, including electroanalytical sensing and electrocatalysis. The electrical conductivity supported by metal nodes along with a redox active organic framework [5-7] enables the electrosynthesis of a wide variety of MOFs [8, 9]. Various chemically or electrochemically synthesized MOFs exhibit electrochemical behaviors that make them potentially useful for stable and selective sensing of various analytes [10-16].

We recently showed that a copper-based MOF (HKUST-1[17]) can be electrochemically synthesized inside an open carbon nanopipette (CNP, *i.e.*, a pulled quartz nanopipette with a carbon-coated inner wall) to prepare the first MOF-based electrochemical nanosensor [18]. The easy to fabricate MOF/CNP nanoelectrodes showed a good sensitivity to H₂O₂. An anticipated drawback of this sensor is that the measured current is due to peroxide reduction, so that the solution needs to be degassed to avoid potential interference of dissolved dioxygen. The oxygen removal from solution may not be straightforward, especially in biological systems. In

this Communication, we carry out the electrodeposition of a cobalt-based MOF (CoMOF) into a CNP to produce a nanoelectrode for oxidation of hydrogen peroxide. The high coordination numbers of Co^(II)/Co^(III) improve the electrochemical response and physical stability of the electrosynthesized nanostructure. 1,3,5-benzenetricarboxylic acid (H₃BTC) was used as the organic linker that readily coordinates the Co^(II) ion upon deprotonation [19], forming a -COO⁻Co^(II)-OOC- framework which is stable during oxidation/reduction of the cobalt nodes. CoMOF has previously been synthesized via chemical [19], or hydrothermal [20] methods using H₃BTC as a ligand. Here, we report the first use of electrosynthesis to directly fabricate a CoMOF/CNP nanosensor for hydrogen peroxide.

Experimental

Chemicals. Cobalt (II) nitrate trihydrate (99%, ACROS), sodium nitrate (J. T. Baker), monosodium phosphate and disodium phosphate (FisherBiotech), 1,3,5-benzentricarboxilic acid (98%, ACROS), nitric acid (70%, Sigma-Aldrich), hexadecyltrimethyl ammonium bromide (98%, ACROS), absolute ethanol (Supelco), hydrogen peroxide (35% w/w aq. solution, Alfa Aesar), Argon gas (99.999%), and methane (99.7%) were used as received. Aqueous solutions were prepared using deionized water from the Milli-Q Advantage A10 system equipped with Q-Gard T2 Pak, a Quantum TEX cartridge, and a VOC pak.

Instrumentation and procedures. All electrochemical experiments were conducted using a CHI model 600E potentiostat (CH Instruments, Austin, TX) inside a Faraday cage. A three-electrode configuration was used with either a 3-mm-diameter GCE or a CNP working electrode, Ag/AgCl reference, and a Pt coil counter electrode. Transmission electron microscopy (TEM) images were obtained using a JEOL model JEM-2100 instrument. A CNP and/or a CNP-CoMOF nanoelectrode was attached to the TEM grid (PELCO Hole Grids, copper) to make its tip visible in the grid center hole, and the rest of the pipette was cut off. A relatively low electron beam voltage of 80 kV was used to avoid damage to the nanoelectrodes. To obtain SEM images, the electrodeposited CoMOF material was transferred to a carbon tape. Scanning electron microscopy—energy dispersive X-ray (SEM-EDX) images and elemental traces were obtained using a Hitachi model S-2600N instrument at 15 KV beam voltage.

Fabrication of open carbon nanopipettes. CNPs were prepared according to the previously reported protocol [18, 21]. Briefly, open nanopipettes were prepared by pulling quartz capillaries (1.0 mm o.d., 0.5/0.7 mm i.d.; Sutter Instrument Company) with a laser pipette puller (P-2000, Sutter Instruments). A thin layer of carbon was deposited on the inner wall of a nanopipette by chemical vapor deposition (Argon/Methane: 3/5) at 950°C for 20 min, as described previously [21]. After gradual cooling, the CNP geometry was examined using TEM. The appropriate protection was used to avoid electrostatic damage to CNPs and nanoelectrodes.

Electrode modification with CoMOF. CoMOF electrosynthesis was conducted according to the previously published protocol [18] with some modifications. Cobalt (II) nitrate trihydrate (4.5 mmol) and sodium nitrate (100 mmol) were dissolved in 5 mL of water (solution A). Then, 2.7 mmol of 1,3,5-benzentricarboxilic acid, and 2.5 mmol of hexadecyltrimethyl ammonium bromide (CTAB), were dissolved in 5 mL of ethanol (solution B). Both A and B

solutions were sonicated for 15 min before mixing under fast stirring. Nitric acid was added dropwise under stirring to adjust the solution pH to ~2.0. The mixture was further stirred for 2 h and degassed before electrodeposition. The resulting solution was used to electrosynthesize CoMOF on a 3-mm-diameter GCE or inside a CNP by applying a potential of –1.4 V vs. Ag/AgCl for 30 min or 50 s, respectively [18]. To remove the residual electrolyte the prepared electrode was immersed in pure water for 10 s. Finally, CTAB was removed from the CoMOF-modified electrode by immersing it in the 1:1 ethanol: water mixture for 1 hour (GCE) or 15 min (CNP) under slow stirring. The prepared electrodes were dried at room temperature for 15 min before electrochemical experiments [22].

Results and Discussion

To validate our approach, we first electrosynthesized and in-situ deposited the film of CoMOF on the surface of a 3 mm glassy carbon electrode (GCE). A cyclic voltammogram (CV) of electrodeposited CoMOF on the GCE electrode in 0.1 M phosphate buffer (PB) solution (**Figure 1a**) shows a pair of a peaks corresponding to oxidation/reduction of $Co^{(II)}/Co^{(III)}$ with the formal potential, $E^{\text{ot}} \approx 0.83 \text{ V vs. Ag/AgCl}$. This value is significantly less positive than the standard potential of the $Co^{(II)}/Co^{(III)}$ couple in aqueous solution, presumably because these species are complexed and embedded into the MOF structure. Similar potential values were reported for the same CoMOF synthesized via a hydrothermal method [20].

[Figure 1]

We employed scanning electron microscopy (SEM) for characterization of the CoMOF morphology and elemental analysis. SEM images of CoMOF (**Figure 1b** and **1c**) reveal its porous structure. The elemental analysis was performed using X-ray energy dispersive technique (SEM-EDX). **Figure 1d** presents the elemental survey of the selected area shown in the red box in panel b, and the maps of each essential element, i.e., carbon, oxygen, and cobalt, are displayed in **Figure 1e-1g**. These maps show that C, O, and Co are distributed uniformly within the sample area.

It has previously been shown that MOF nanostructures are suitable for sensing various analytes, including drugs and biologically important species [23-28]. We used CoMOF electrodeposition to modify CNPs and produce nanoelectrodes for H_2O_2 oxidation. (For details, see the experimental section). **Figure 2a** shows a representative CV of a CNP in 0.1 M phosphate buffer solution (pH 7.1) containing 1 mM ferrocenemethanol (FcMeOH) that was recorded before CoMOF deposition at a scan rate of 100 mV/s. A pair of essentially symmetrical voltammetric peaks with the half-peak potential ~130 mV vs Ag/AgCl reference corresponds to oxidation/reduction of FcMeOH molecules inside the CNP cavity [29]. At more positive potentials ($E > \sim 0.3$ V), the diffusion-limited steady-state current is due to the oxidation of the same species at the carbon-coated CNP orifice. Eq. (1) is a good approximation for the diffusion steady state current: [29]

$$i_{ss} = 4nFDca \tag{1}$$

where, n = 1 is the number of transferred electrons, F is the Faraday constant, $D = 7.6 \times 10^{-6}$ cm²/s [30] and c = 1 mM are the diffusion coefficient and bulk concentration of FcMeOH, respectively, and a is the radius of the CNP orifice. The i_{ss} value of 36.7 pA, in **Figure 2a** corresponds to the apparent CNP radius, $a \sim 121$ nm.

The electrosynthesis of CoMOF inside a CNP was carried out in the same solution that was used to deposit it on a GCE, but the deposition time was shorter, *i.e.*, 50 s. The nanostructure formed during electrodeposition of CoMOF into the CNP blocked its orifice, preventing the FcMeOH diffusion into the pipette cavity. Accordingly, the voltammogram of FcMeOH at a CNP–CoMOF electrode (**Figure 2b**) is sigmoidal rather that peak-shaped. The well-defined steady-state diffusion-limited current of FcMeOH at this modified electrode is very similar to the *iss* value before CoMOF deposition, and essentially the same radius can be found from Eq. (1). This finding is similar to that in our previous paper on CuMOF-CNP [18], except for a better shape of the voltammogram in **Figure 2b**, which may be due to a higher conductivity of CoMOF.

[Figure 2]

Further characterization of the CNP–CoMOF was performed using electron microscopy techniques, including transmission electron microscopy (TEM) and scanning electron microscopy (SEM). The TEM image of a CNP–CoMOF in **Figure 3a** supports the blockage of the CNP tip by electrodeposited CoMOF. MOF fills a few micrometer-long part of the CNP adjacent to its orifice. Although the solution can enter the porous structure of CoMOF (**Figure 1b**), the oxidation of FcMeOH to Fc+MeOH occurs at about 0.2 V vs. Ag/AgCl (**Figure 2b**), whereas the Co^(II) sites are oxidized at much higher potentials (~0.8 V; **Figure 1a**). Therefore, the oxidation of FcMeOH at CNP-CoMOF electrodes occurs at the carbon ring exposed to the solution rather than by electron transfer to CoMOF.

The composition of CoMOF deposited into a CNP was revealed by SEM-EDX. A cross section SEM image of the CNP-CoMOF, where the corresponding SEM-EDX elemental spectrum was collected, is shown in **Figure 3b**. The SEM-EDX spectrum (**Figure 3c**) supports the presence of cobalt, oxygen, and carbon as the main components of the CoMOF, while the absence of nitrogen confirms the essentially complete removal of CTAB during the washing step.

[Figure 3]

MOF-coated electrodes have previously been used as electrochemical sensors [13, 15, 31-33] and nanosensors [18] for various important analytes. CVs of a CNP-CoMOF were recorded in the presence of different concentrations of hydrogen peroxide in 0.1 M PB solution within the oxidation potential window of 0–1.2 V vs. Ag/AgCl (**Figure 4a**). The half-wave potential of the anodic wave is ~0.97 V. This value is more positive than the mid-peak potential of Co^(II)/Co^(III) (**Figure 1a**) likely due to the combination of a fast mass-transfer rate at a nanometer-sized CNE-CoMOF electrode and slow kinetics of Co^(II) oxidation. This anodic wave is due to the catalytic oxidation of H₂O₂ within the CoMOF porous structure (eq. 2): by electrogenerated Co^(III)

$$2\text{Co}^{(\text{III})} + \text{H}_2\text{O}_2 \rightarrow 2\text{Co}^{(\text{II})} + 2\text{H}^+ + \text{O}_2$$
 (2)

The steady-state diffusion-limited current of hydrogen peroxide oxidation at a disk-type nanoelectrode can be evaluated from eq (1) with n = 2 and $D_{\text{H}_2\text{O}_2} = 1.4 \times 10^{-5} \text{ cm}^2/\text{s}$ [34]. The substitution of $c_{\text{H}_2\text{O}_2} = 10 \text{ mM}$ and a = 121 nm (determined above) in eq (1) yields the expected diffusion-limited current value, $i_{\text{ss}} = 1.5 \text{ nA}$, i.e., about 30 times the plateau current in curve 4 (**Figure 4a**) obtained for the oxidation of 10 mM H₂O₂. Clearly, the plateau current in **Figure 4a** is kinetic rather than diffusion controlled. Although the mechanism of the catalytic oxidation of peroxide (reaction 2) is complicated, the kinetic limiting current can be expressed as:

$$i_k = k_{\rm nFAC_{Co(III)}C_{H2O2}}$$
 (3)

where A is the surface area of MOF-modified CNE exposed to the solution, k is the effective rate constant of reaction (2), and $C_{Co(III)}$ is the surface concentration of $Co^{(III)}$ species. This equation predicts that the plateau current in **Figure 4a** should be directly proportional to H_2O_2 concentration. The linear experimental calibration curve shown in **Figure 4b** agrees with this prediction and suggests the possibility of a H_2O_2 sensor based on its oxidation at CNP–CoMOF nanoelectrode. The limit of detection (LOD) was calculated to be 1.05 mM for three replicates (n = 3) measured with the same electrode under the same experimental conditions.

[Figure 4]

Conclusions

In conclusion, we demonstrated that an electrochemical nanosensor for hydrogen peroxide detection can be readily fabricated by electrodepositing CoMOF into a CNP. The response of the resulting electrode is mediated by the Co^(II)/Co^(III) redox couple with the locally electrogenerated Co^(III) species oxidizing hydrogen peroxide. An important advantage of this sensor is that it is not sensitive to dissolved oxygen and does not require solution degassing, which may not always be feasible, e.g., in biological systems. It would be interesting to explore the applicability of the CNE-CoMOF nanosensor to detection of reactive oxygen and nitrogen species other than H₂O₂ (e.g., NO, nitrite, and peroxynitrite ions). This platform may also be extended to other types of MOFs, where metal nodes or organic ligands (or both) can react with a target analyte; however, practical applications of such nanosensors would require improvements in response stability and reproducibility.

Acknowledgements

The support of this work by the National Science Foundation grant CHE-2102298 is gratefully acknowledged. M.H. appreciates Ms. Lisa Hlinka's help with collecting SEM-EDX images.

References

- [1] K. Suresh, A. P. Kalenak, A. Sotuyo and A. J. Matzger, Metal-Organic Framework (MOF) Morphology Control by Design, Chem. Eur. J., 28, (2022) e202200334.
- [2] G. Chakraborty, I.-H. Park, R. Medishetty and J. J. Vittal, Two-Dimensional Metal-Organic Framework Materials: Synthesis, Structures, Properties and Applications, Chem. Rev., 121, (2021) 3751-3891.
- [3] G. Cai, P. Yan, L. Zhang, H.-C. Zhou and H.-L. Jiang, Metal—Organic Framework-Based Hierarchically Porous Materials: Synthesis and Applications, Chem. Rev., 121, (2021) 12278-12326.
- [4] P.-L. Wang, L.-H. Xie, E. A. Joseph, J.-R. Li, X.-O. Su and H.-C. Zhou, Metal—Organic Frameworks for Food Safety, Chem. Rev., 119, (2019) 10638-10690.
- [5] H. T. B. Pham, J. Y. Choi, S. Huang, X. Wang, A. Claman, M. Stodolka, S. Yazdi, S. Sharma, W. Zhang and J. Park, Imparting Functionality and Enhanced Surface Area to a 2D Electrically Conductive MOF Via Macrocyclic Linker, J. Am. Chem. Soc., 144, (2022) 10615-10621.
- [6] L. B. Zasada, L. Guio, A. A. Kamin, D. Dhakal, M. Monahan, G. T. Seidler, C. K. Luscombe and D. J. Xiao, Conjugated Metal-Organic Macrocycles: Synthesis, Characterization, and Electrical Conductivity, J. Am. Chem. Soc., 144, (2022) 4515-4521.
- [7] M. Ko, L. Mendecki and K. A. Mirica, Conductive Two-Dimensional Metal—Organic Frameworks as Multifunctional Materials, Chem. Commun., 54, (2018) 7873-7891.
- [8] H. Al-Kutubi, J. Gascon, E. J. R. Sudhölter and L. Rassaei, Electrosynthesis of Metal—Organic Frameworks: Challenges and Opportunities, ChemElectroChem, 2, (2015) 447-447.
- [9] V. M. V and G. Nageswaran, Review–Direct Electrochemical Synthesis of Metal Organic Frameworks, J. Electrochem. Soc., 167, (2020) 155527.
- [10] C.-H. Chuang and C.-W. Kung, Metal—Organic Frameworks toward Electrochemical Sensors: Challenges and Opportunities, Electroanalysis, 32, (2020) 1885-1895.
- [11] Y. Chang, J. Lou, L. Yang, M. Liu, N. Xia and L. Liu, Design and Application of Electrochemical Sensors with Metal—Organic Frameworks as the Electrode Materials or Signal Tags, Nanomaterials, 12, (2022) 3248.
- [12] L.-T. Zhang, Y. Zhou and S.-T. Han, The Role of Metal-Organic Frameworks in Electronic Sensors, Angew. Chem. Ed. Int., 133, (2021) 15320-15340.

- [13] S. Tajik, H. Beitollahi, F. Garkani Nejad, I. Sheikhshoaie, A. S. Nugraha, H. W. Jang, Y. Yamauchi and M. Shokouhimehr, Performance of Metal—Organic Frameworks in the Electrochemical Sensing of Environmental Pollutants, J. Mater. Chem. A, 9, (2021) 8195-8220.
- [14] S. Pal, S.-S. Yu and C.-W. Kung, Group 4 Metal-Based Metal—Organic Frameworks for Chemical Sensors, Chemosensors, 9, (2021) 306-337.
- [15] J. F. Olorunyomi, S. T. Geh, R. A. Caruso and C. M. Doherty, Metal–Organic Frameworks for Chemical Sensing Devices, Mater. Horiz., 8, (2021) 2387-2419.
- [16] L.-L. Gao and E.-Q. Gao, Metal–Organic Frameworks for Electrochemical Sensors of Neurotransmitters, Coord. Chem. Rev., 434, (2021) 213784.
- [17] S. S. Y. Chui, S. M. F. Lo, J. P. H. Charmant, A. G. Orpen and I. D. Williams, A Chemically Functionalizable Nanoporous Material [Cu₃(TMA)₂(H₂O)₃]_n, Science, 283, (1999) 1148-1150.
- [18] M. Hesari, R. Jia and M. V. Mirkin, Metal-Organic-Framework-Based Electrochemical Nanosensor for Hydrogen Peroxide, ChemElectroChem, 9, (2022) e202200373.
- [19] A. Karmakar and C. L. Oliver, A Two-Dimensional Metal Organic Network with 1,3,5-Benzenetricarboxylate and Cobalt (II) Ions: Synthesis, Structure and Topology, Z. Kristallogr., 228, (2013) 330-334.
- [20] D. Ge, J. Peng, G. Qu, H. Geng, Y. Deng, J. Wu, X. Cao, J. Zheng and H. Gu, Nanostructured Co(II)-Based Mofs as Promising Anodes for Advanced Lithium Storage, New J. Chem., 40, (2016) 9238-9244.
- [21] K. Hu, Y. Wang, H. Cai, M. V. Mirkin, Y. Gao, G. Friedman and Y. Gogotsi, Open Carbon Nanopipettes as Resistive-Pulse Sensors, Rectification Sensors, and Electrochemical Nanoprobes, Anal. Chem., 86, (2014) 8897-8901.
- [22] N. Nioradze, R. Chen, J. Kim, M. Shen, P. Santhosh and S. Amemiya, Origins of Nanoscale Damage to Glass-Sealed Platinum Electrodes with Submicrometer and Nanometer Size, Anal. Chem., 85, (2013) 6198-6202.
- [23] S. Gutiérrez-Tarriño, J. L. Olloqui-Sariego, J. J. Calvente, M. Palomino, G. Mínguez Espallargas, J. L. Jordá, F. Rey and P. Oña-Burgos, Cobalt Metal—Organic Framework Based on Two Dinuclear Secondary Building Units for Electrocatalytic Oxygen Evolution, ACS Appl. Mater. Interfaces, 11, (2019) 46658-46665.
- [24] X.-M. Tian, S.-L. Yao, C.-Q. Qiu, T.-F. Zheng, Y.-Q. Chen, H. Huang, J.-L. Chen, S.-J. Liu and H.-R. Wen, Turn-on Luminescent Sensor toward Fe³⁺, Cr³⁺, and Al³⁺ Based on a

- Co(II) Metal-Organic Framework with Open Functional Sites, Inorg. Chem., 59, (2020) 2803-2810.
- [25] L. Ji, J. Wang, K. Wu and N. Yang, Tunable Electrochemistry of Electrosynthesized Copper Metal–Organic Frameworks, Adv. Func. Mater., 28, (2018) 1706961.
- [26] P. Hu, X. Zhu, X. Luo, X. Hu and L. Ji, Cathodic Electrodeposited Cu-BTC MOFs Assembled from Cu(II) and Trimesic Acid for Electrochemical Determination of Bisphenol A, Microchimica Acta, 187, (2020) 145.
- [27] M. Ko, L. Mendecki, A. M. Eagleton, C. G. Durbin, R. M. Stolz, Z. Meng and K. A. Mirica, Employing Conductive Metal–Organic Frameworks for Voltammetric Detection of Neurochemicals, J. Am. Chem. Soc., 142, (2020) 11717-11733.
- [28] M. Sohail, M. Altaf, N. Baig, R. Jamil, M. Sher and A. Fazal, A New Water Stable Zinc Metal Organic Framework as an Electrode Material for Hydrazine Sensing, New J. Chem., 42, (2018) 12486-12491.
- [29] Y. Yu, J.-M. Noël, M. V. Mirkin, Y. Gao, O. Mashtalir, G. Friedman and Y. Gogotsi, Carbon Pipette-Based Electrochemical Nanosampler, Anal. Chem., 86, (2014) 3365-3372.
- [30] Y. Yu, T. Sun and M. V. Mirkin, Toward More Reliable Measurements of Electron-Transfer Kinetics at Nanoelectrodes: Next Approximation, Anal. Chem., 88, (2016) 11758-11766.
- [31] X. Zhang, K. Wan, P. Subramanian, M. Xu, J. Luo and J. Fransaer, Electrochemical Deposition of Metal–Organic Framework Films and Their Applications, J. Mater. Chem. A, 8, (2020) 7569-7587.
- [32] Z. Zeng, X. Fang, W. Miao, Y. Liu, T. Maiyalagan and S. Mao, Electrochemically Sensing of Trichloroacetic Acid with Iron(II) Phthalocyanine and Zn-Based Metal Organic Framework Nanocomposites, ACS Sensors, 4, (2019) 1934-1941.
- [33] T.-E. Chang, C.-H. Chuang and C.-W. Kung, An Iridium-Decorated Metal—Organic Framework for Electrocatalytic Oxidation of Nitrite, Electrochem. Commun., 122, (2021) 106899.
- [34] S. A. M. van Stroe-Biezen, F. M. Everaerts, L. J. J. Janssen and R. A. Tacken, Diffusion Coefficients of Oxygen, Hydrogen Peroxide and Glucose in a Hydrogel, Anal. Chim. Acta, 273, (1993) 553-560.

Figure Captions

Figure 1. Electrochemistry and SEM characterization of CoMOF. (a) Cyclic voltammogram of electrodeposited CoMOF on GCE in 0.1 M PB. Potential scan rate, v = 100 mV/s. (b) SEM image of a CoMOF sample. The scale bar is 8 μ m. (c) Zoomed-in image of the sample area labeled by the dashed rectangle in panel b. The scale bar is 5 μ m. (d) Elemental survey of the selected area shown in panel b. The insets display SEM-EDX maps of carbon (e), oxygen (f), and cobalt (g) in the selected area.

Figure 2. (a) Cyclic voltammogram of 1 mM ferrocenemethanol in 0.1 M phosphate buffer (pH = 7.1) at an ~200 nm CNP (the steady-state current is shown by a double-sided arrow), and (b) steady-state voltammogram of the same CNP modified with CoMOF in the same solution. v = 100 mV/s.

Figure 3. (a) TEM image of a CNP-CoMOF. (b) A side view image of the CoMOF-CNP section from which the data shown in panel (c) was collected along the green line. (c) SEM energy dispersion X-ray (SEM-EDX) elemental spectrum of the CNP-CoMOF tip.

Figure 4. (a) Cyclic voltammograms of CNP-CoMOF in the absence (1) and in the presence of 1 mM (2), 5 mM (3), 10 mM (4), and 20 mM (5) of H_2O_2 in 0.1 M phosphate buffer. v = 50 mV/s. The dashed line corresponds to the potential at which the calibration shown in panel **b** was obtained. (b) Concentration dependence of the H_2O_2 plateau current extracted from the CVs shown in panel (a) at E = 1.1 V vs. Ag/AgCl. Error bars in (b) are standard deviations for n=3.

Figure 1

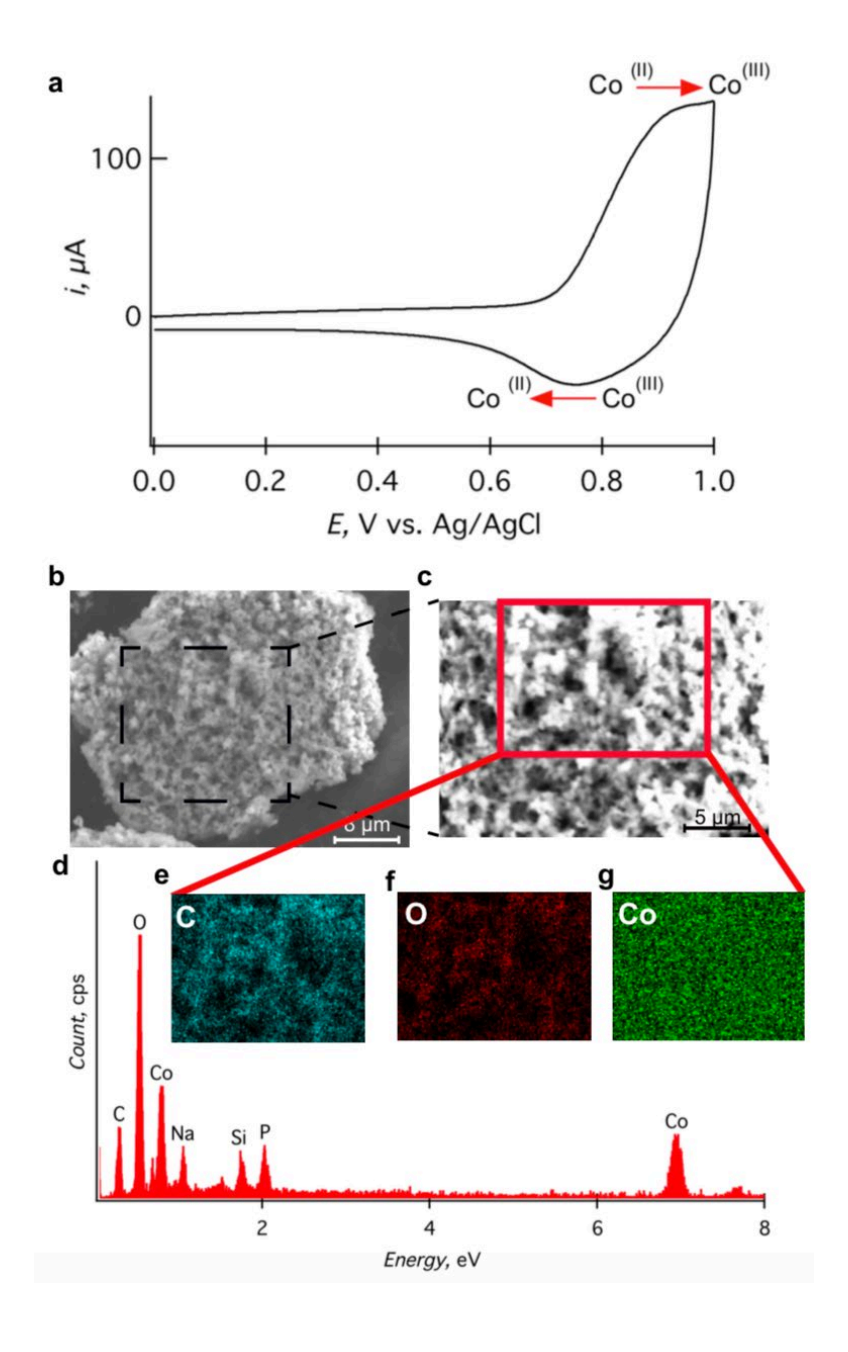


Figure 2

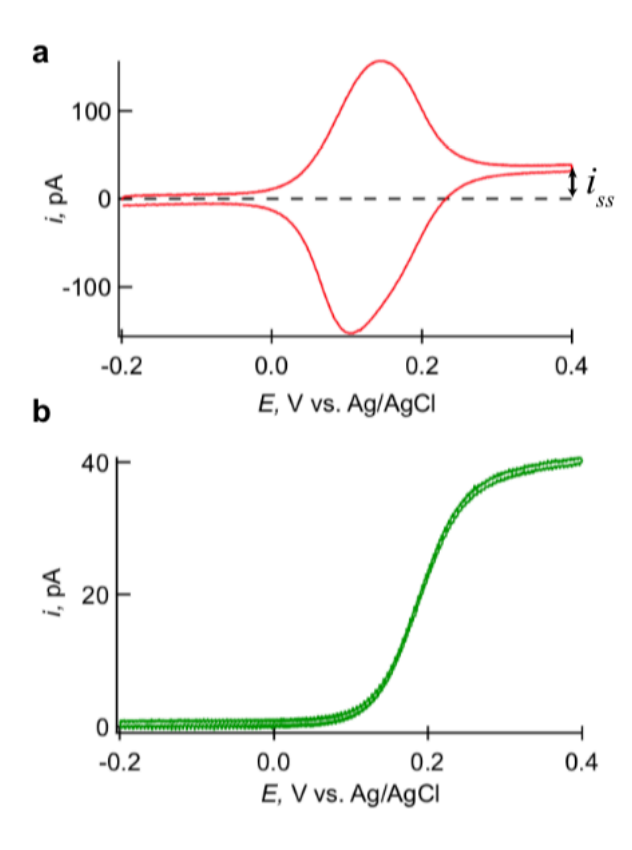


Figure 3

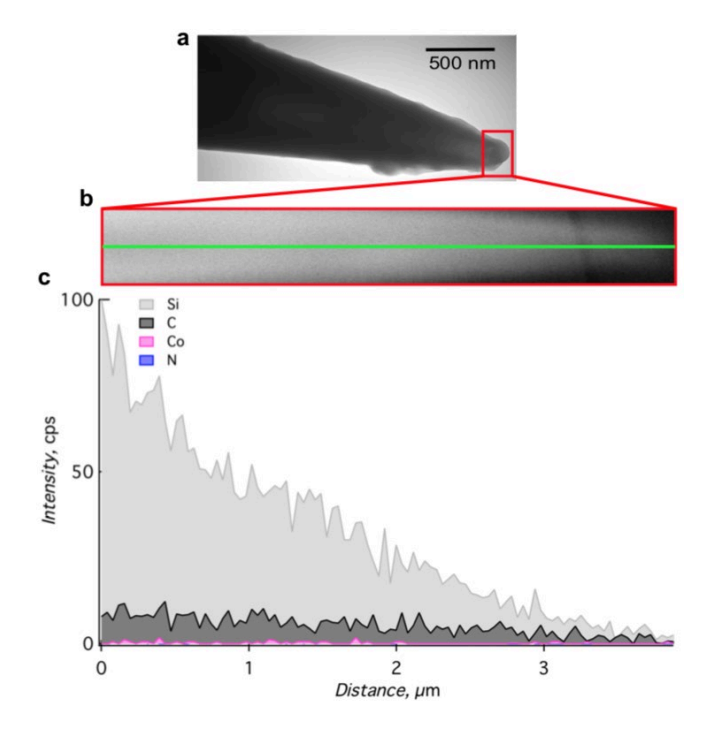


Figure 4

